Published in final edited form as:
Biomacromolecules. 2006 November ; 7(11): 3188–3195. doi:10.1021/bm060559c.

Force Spectroscopy of LFA-1 and Its Ligands, ICAM-1 and ICAM-2

Ewa P. Wojcikiewicz[*], **Midhat H. Abdulreda**, **Xiaohui Zhang**[‡], and **Vincent T. Moy**
Department of Physiology and Biophysics, University of Miami Miller School of Medicine, Miami, Florida 33136

Abstract

Single-molecule measurements of the interaction of leukocyte function-associated antigen-1 (LFA-1), expressed on Jurkat T cells, with intercellular adhesion molecules-1 and -2 (ICAM-1 and ICAM-2) were conducted using atomic force microscopy (AFM). The force spectra (i.e., unbinding force versus loading rate) of both the LFA-1/ICAM-1 and LFA-1/ICAM-2 interactions were acquired at a loading rate range covering 3 orders of magnitude (50–60 000 pN/s) and revealed a fast loading regime and a slow loading regime. This indicates that the dissociation of both complexes involves overcoming a steep inner and a wide outer activation barrier. LFA-1 binding to ICAM-1 and ICAM-2 was strengthened in the slow loading regime by the addition of Mg^{2+}. Differences in the dynamic strength of the LFA-1/ICAM-1 and LFA-1/ICAM-2 interactions can be attributed to the presence of wider barriers in the ICAM-2 complex, making it more responsive to a pulling force than the ICAM-1 complex.

Introduction

The interaction of leukocyte function-associated antigen-1 (LFA-1, $\alpha_L\beta_2$) integrin with intercellular adhesion molecule-1 (ICAM-1, CD54) and ICAM-2 (CD109) contributes to cell adhesion during leukocyte homing.[1] LFA-1 is a heterodimeric transmembrane glycoprotein expressed on leukocytes.[2] ICAM-1 and ICAM-2 are composed of five and two immunoglobulin (Ig) domains, respectively, a transmembrane domain, and a short cytoplasmic domain. Both ICAM-1 and ICAM-2 have been shown to be involved in cell transmigration across the unstimulated endothelium, either by having overlapping functions or working in concert.[3-5] On the unstimulated endothelium, ICAM-2 is constitutively expressed at much higher levels than ICAM-1 and is the dominant receptor responsible for mediating leukocyte trafficking under normal conditions.[6] This changes as ICAM-1 expression is up-regulated by inflammatory mediators and cytokines and ICAM-1 becomes largely responsible for mediating the adhesion of leukocytes to the inflamed endothelium.[7]

Binding of LFA-1 is localized to the first immunoglobulin domain of both ICAM-1 and ICAM-2.[8] Both ICAMs bind to the extracellular globular headpiece of LFA-1. More specifically, the ICAM-1 and ICAM-2 binding site has been localized to the metal ion dependent adhesion site (MIDAS) of the α subunit I domain. The key residues required for ICAM-1 and ICAM-2 binding to LFA-1 were identified to be Glu-34 of ICAM-1 and Glu-37 of ICAM-2.[9] These acidic residues complete the coordination of Mg^{2+} in the MIDAS of the I domain upon ligand binding.[10-12] Structural and mutational studies also revealed that a ring of hydrophobic amino acids surrounding the MIDAS of the I domain plays an important role in LFA-1 binding.[13] These amino acids interact with complementary hydrophobic rings on ICAM-1 and ICAM-2.

[*]Corresponding author. Phone: (305) 243-3201. Fax: (305) 243-5931. E-mail: ewojcikiewicz@med.miami.edu.
[‡]Present address: CBR institute for Biomedical Research, Harvard Medical School, Boston, MA 02115.

Leukocyte adhesion is enhanced by affinity and avidity modulation of LFA-1 upon cell activation. Affinity modulation is induced by inside-out signaling in vivo and can be mimicked in vitro by treatment with Mg^{2+}/EGTA, leading to the expression of a high-affinity conformer of LFA-1. This process is associated with the downward displacement of the C-terminal α7 helix of the LFA-1 I domain that results in the opening of the ligand binding site.[14-19] Avidity modulation is associated with elevated levels of intracellular calcium, resulting in cytoskeletal rearrangement and lateral redistribution of LFA-1. Enhanced adhesion following avidity modulation results from a greater availability of receptors for ligand binding. Experimentally, avidity modulation can be induced by phorbol myristate acetate (PMA), which activates protein kinase C (PKC). This leads to the increase of intracellular calcium as well as the activation of calpain protease, which cleaves LFA-1 from the constraints of the cytoskeleton, thus allowing it to redistribute on the cell surface.

Although the interactions of LFA-1 with ICAM-1 and ICAM-2 are structurally and functionally similar, LFA-1 binds to ICAM-1 with a 5-fold higher affinity than ICAM-2 as measured by competitive binding assays and surface plasmon resonance.[6,14] In the current study, single-molecule atomic force microscopy (AFM) measurements were carried out to determine the effects of a pulling force on the unbinding of LFA-1/ICAM-1 and LFA-1/ICAM-2 complexes. These measurements revealed the dissociation pathways of the two complexes for both low- and high-affinity conformers of LFA-1.

Experimental Section

Cells and Reagents

The Jurkat cell line was maintained in continuous culture in RPMI 1640 medium supplemented with 10% heat-inactivated fetal calf serum (Irvine Scientific, Santa Ana, CA), penicillin (50 U/mL, Gibco BRL, Grand Island, NY), and streptomycin (50 μg/mL, Gibco BRL). The cells were expanded on a 3-day cycle.[20]

ICAM-1.Fc and ICAM-2.Fc were purchased from R & D Systems, Inc. (Minneapolis, MN). The ICAM-1.Fc chimera consisted of all five extracellular Ig domains of human ICAM-1 (Met 1 to Glu 48) and the Fc fragment of human IgG_1. ICAM-2.Fc has both extracellular Ig domains of human ICAM-2 and the Fc fragment of human IgG_1. Monoclonal antibodies against ICAM-1 (clone BBIG-I1) and ICAM-2 (clone 86911) were also purchased from R & D Systems, Inc. Antibody against LFA-1 (clone TS1.22) was purified from culture supernatant of TS1.22 hybridoma cells (ATCC, Manassas, VA) by protein A affinity chromatography.

To induce expression of the high-affinity form of LFA-1, Jurkat cells were activated with 5 mM $MgCl_2$ and 1 mM EGTA. To promote cell adhesion via avidity modulation, the Jurkat cells were treated with 100 nM PMA from a stock solution of 1 mM in dimethyl sulfoxide (DMSO).

Protein Immobilization

A 20 μL aliquot of ICAM-1.Fc or ICAM-2.Fc at 20 μg/mL (single-molecule experiments) or 50 μg/mL (whole-cell experiments) in 0.1 M $NaHCO_3$ (pH 8.6) was adsorbed overnight at 4 °C on the center of a 35 mm tissue culture dish (Falcon 353001, Becton Dickinson Labware, Franklin Lakes, NJ). Unbound protein was removed by washing with phosphate buffered saline (PBS, 10 mM PO_4^{3-}, 150 mM NaCl, pH7.3). The exposed surface of the dish was blocked using 100 μg/mL bovine albumin (Sigma) in PBS to eliminate nonspecific binding to the dish surface. One coated dish is used to complete each AFM experiment. Approximately 3000 measurements were typically acquired over 6–8 h during the experiments. No decrease in the adhesion frequency was observed.

AFM Measurements of Adhesion Forces

An apparatus designed to be operated in force spectroscopy mode was used to perform the AFM force measurements.[21-23] Concanavalin A (Con A)-mediated linkages were used to attach Jurkat cells to the AFM cantilever.[24] To prepare the Con A-functionalized cantilever, the cantilevers were soaked in acetone for 5 min, UV-irradiated for 30 min, and incubated in biotinamidocaproyl-labeled bovine serum albumin (biotin-BSA, 0.5 mg/mL in 100 mM $NaHCO_3$, pH 8.6; Sigma) overnight at 37 °C. The cantilevers were then rinsed 3 times with PBS and incubated in streptavidin (0.5 mg/mL in PBS; Pierce, Rockford, IL) for 10 min at room temperature. Unbound streptavidin was removed by rinsing in PBS. The cantilevers were then incubated in biotinylated Con A (0.2 mg/mL in PBS; Sigma) and rinsed again with PBS prior to use. The strength of the Con A interaction with the cell had been previously measured and was found to be >2 nN, which is much greater than the forces being measured for the LFA-1/ICAM-1 and LFA-1/ICAM-2 interactions, which are in the piconewton range.

A single Jurkat cell was attached to the cantilever by positioning the end of the Con A-functionalized cantilever above the center of the cell and carefully lowering it onto the cell for approximately 1 s. When attached, the cell was positioned right behind the AFM tip of the cantilever, as illustrated in Figure 1.[24,25]

The cantilever with an attached Jurkat cell was lowered onto the sample using a piezoelectric translator. The interaction between the attached cell and the sample was derived from the deflection of the cantilever, which was measured by reflecting a laser beam off the cantilever onto a position-sensitive two-segment photodiode detector. AFM cantilevers were purchased from Veeco (MLCT-AUHW, Veeco Probes, Santa Barbara, CA). The largest triangular cantilever (320 μm long and 22 μm wide) from a set of five on the cantilever chip was used in our measurements. These cantilevers were calibrated by analysis of their thermally induced fluctuation to determine their spring constant.[26] The experimentally determined spring constants were consistent with the nominal value of 10 mN/m specified by the manufacturer.

Whole Cell Adhesion Studies

To obtain multiple-bond interactions between the Jurkat cell attached to the AFM cantilever and the ICAM-1 or ICAM-2 protein coated on a dish, an indentation force of ~200 pN and 2 s contact time were used. The experiments were carried out at a cantilever retraction rate of 5 μm/s at 25 °C.

AFM Force Measurements of Individual LFA-1/ICAM-1 and LFA-1/ICAM-2 Interactions

Contact time and indentation force were minimized between the Jurkat cell and the sample in order to obtain measurements of unitary LFA-1/ICAM-1 and LFA-1/ICAM-2 unbinding forces. An adhesion frequency of <30% in the force measurements ensured that there is a >85% probability that the adhesion event is mediated by a single LFA-1/ICAM-1 bond.[24] AFM measurements were collected at cantilever retraction speeds ranging from 0.1 to 26 μm/s to achieve the desired loading rates (~50–60 000 pN/s). Since the hydrodynamic damping coefficient of the cantilever in water is 2 pN•s/μm, measurements collected at retraction speeds greater than 1 μm/s were corrected for hydrodynamic drag.[27,28] All experiments were carried out at 25 °C.

Dynamic Force Spectroscopy

According to the Bell model, a pulling force, *f*, distorts the intermolecular potential of a ligand–receptor complex, leading to the lowering of the activation energy and an increase of the dissociation rate $k(f)$ as follows:

$$k(f) = k^{\circ} \exp[f\gamma/k_B T] \quad (1)$$

where k° is the dissociation rate constant in the absence of a pulling force, γ is the position of the transition state, T is the absolute temperature, and k_B is the Boltzmann constant. For a constant loading rate r_f, the probability density for the unbinding of the complex as a function of the pulling force f is given by[29]

$$P(f) = k^\circ \exp\left\{\frac{\gamma f}{k_B T}\right\} \exp\left\{\frac{k^\circ k_B T}{\gamma r_f}\left[1 - \exp\left(\frac{\gamma f}{k_B T}\right)\right]\right\} \quad (2)$$

with the most probable unbinding force f^* given by

$$f^* = \frac{k_B T}{\gamma} \ln\left\{\frac{\gamma}{k^\circ k_B T}\right\} + \frac{k_B T}{\gamma} \ln\{r_f\} \quad (3)$$

Hence, the Bell model predicts that the most probable unbinding force f^* is a linear function of the logarithm of the loading rate. Experimentally, f^* was determined from the mode of the unbinding force histograms. The Bell model parameters were determined by fitting eq 3 to the plot of f^* versus $\ln(r_f)$.

Results

AFM Force Measurements of the LFA-1/ICAM-1 and LFA-1/ICAM-2 Interactions

Direct force measurements of the adhesive interaction between a Jurkat cell and immobilized ICAM-1 and ICAM-2 were carried out by AFM. As described in Experimental Section, the Jurkat cell was coupled to the end of an AFM cantilever and either ICAM-1 or ICAM-2 was immobilized on the surface of a tissue culture dish (Figure 1). Figure 2A presents a series of AFM measurements acquired under conditions that favored the formation of multiple LFA-1/ICAM-1 bonds upon cell/substrate contact. As evident from these measurements, the separation of the attached cell from the ICAM-1-coated surface is a complex process with multiple sudden jumps in force. These force transitions can be attributed to the breakage of the LFA-1/ICAM-1 bonds formed between the cell and the ICAM-1-coated surface. In many instances, the measurements revealed that the cell undergoes a large deformation before the last linkage is severed.

The top two traces of Figure 2A show that the interaction between a resting Jurkat cell and immobilized ICAM-1 is inhibited by an anti-ICAM-1 antibody. Cell adhesion in the AFM measurements is quantified by the work done by the cantilever to detach the cell from the substrate. This work of de-adhesion was derived from integrating the adhesive force over the distance traveled by the cantilever as highlighted in trace d of Figure 2A. Figure 2B shows that inhibition of ICAM-1 resulted in >80% reduction in cell adhesion as measured by the work of de-adhesion, demonstrating that adhesion is mediated by ICAM-1. In contrast, cell adhesion was enhanced by the addition of either Mg^{2+}/EGTA (trace c) or PMA (trace d). Activation of cells with Mg^{2+}/EGTA has been shown to promote the expression of the high-affinity form of LFA-1.[30,31] Its presence led to a 2-fold increase in the work of de-adhesion in our measurements. To investigate the role of avidity modulation in leukocyte adhesion, we treated the Jurkat cells with PMA, a potent PKC activator that induces receptor clustering on the cell surface as well as cell spreading.[16,32-35] As shown in Figure 2, PMA-stimulated Jurkat cells adhered significantly more strongly to ICAM-1 than the unstimulated cells as is evident by the 4-fold increase in the work of de-adhesion following stimulation.

To better understand the role of ICAM-1 and ICAM-2 in leukocyte adhesion, we compared the adhesion of Jurkat cells to immobilized ICAM-1 and ICAM-2. As in the case of ICAM-1, Jurkat adhered specifically to ICAM-2 (Figure 2B). Moreover, adhesion was elevated following treatment with either Mg^{2+}/EGTA or PMA. In general, the Jurkat cell line adhered

better to ICAM-1 than ICAM-2. Our measurements confirm previous findings that ICAM-1 mediates stronger adhesion of leukocytes than ICAM-2.

Dynamic Strength of the LFA-1/ICAM-1 and LFA-1/ICAM-2 Complexes

To characterize the intrinsic properties of the interaction between LFA-1 and its ligands, we carried out single-molecule AFM force measurements. Measurements of the bond strengths of individual LFA-1/ICAM-1 and LFA-1/ICAM-2 complexes were acquired by minimized contact between the Jurkat cell and immobilized ICAM-1 and ICAM-2. The contact duration and compression force of these measurements were ~50 ms and ~100 pN, respectively. Measurements acquired under these conditions have an adhesion frequency of approximately 30%. Examples of these AFM force-displacement traces are presented in Figure 3. The traces observed in these adhesion measurements are consistent with measurements obtained using other cell systems.[21,24,36,37] The breakage of a single LFA-1/ICAM-1 (Figure 3A) or LFA-1/ICAM-2 (Figure 3B) complex in the force-displacement traces is registered by a rapid drop in force following a linear increase in force. The magnitude of the force transition is the unbinding force of the complex. To determine the dynamic response of the LFA-1/ICAM-1 and LFA-1/ICAM-2 complexes, the AFM single-bond measurements were conducted at loading rates of 50–60 000 pN/s. Representative force histograms of the LFA-1/ICAM-1 and LFA-1/ICAM-2 interactions acquired at different loading rates are shown in Figure 4. As evident, the unbinding forces of these complexes are shifted toward higher values with increasing loading rate.[27,38,39]

Using values corresponding to the mode of the force histograms, we plotted dynamic force spectra (DFS) of the human LFA-1/ICAM-1 and LFA-1/ICAM-2 interactions (Figure 5). The DFS (plot of unbinding force vs loading rate) of the LFA-1/ICAM-1 complex displayed a gradual logarithmic increase in unbinding force up to a loading rate of approximately 7000 pN/s (Figure 5A). The unbinding force increased at a faster rate in the second regime (i.e., loading rates > 7000 pN/s). Activation of LFA-1 by Mg^{2+}/EGTA resulted in higher LFA-1/ICAM-1 unbinding forces in the slow loading regime but had no significant impact on the forces in the fast loading regime (i.e., loading rates > 7000 pN/s). Interestingly, activation of Jurkat with PMA did not modify the LFA-1/ICAM-1 DFS (Figure 5A).

This study also explored the LFA-1/ICAM-2 interaction. The unbinding force of the LFA-1/ICAM-2 complex also increased over 3 orders of magnitude of loading rate and exhibited two loading regimes (Figure 5B). Treatment of the cells with both Mg^{2+}/EGTA and PMA resulted in a similar dynamic response of the LFA-1/ICAM-2 complex to that observed for the LFA-1/ICAM-1 complex. Activation with Mg^{2+}/EGTA resulted in elevated forces in the first loading regime, while PMA-stimulated cells and untreated cells had overlapping DFS. However, there are some significant differences in the properties of the LFA-1/ICAM-1 and LFA-1/ICAM-2 complexes that may be important for understanding their function. The most pronounced difference is that the strength of the LFA-1/ICAM-2 complex is significantly weaker than that of the LFA-1/ICAM-1 complex over the entire DFS (Figure 5C). Also, the increase in unbinding force was much more gradual with increasing loading rate for the LFA-1/ICAM-2 complex than for the LFA-1/ICAM-1 complex. This difference was most pronounced in the fast loading regime (i.e. loading rates > 7000 pN/s). Another difference was observed in the response of the two complexes to Mg^{2+}/EGTA activation in the slow loading regimes (i.e., loading rates < 7000 pN/s). The average difference between resting and Mg^{2+}/ EGTA-activated cells was ~25 pN for the LFA-1/ICAM-1 complex and only ~10 pN for the LFA-1/ICAM-2 complex.

Discussion

This work was conducted to characterize the interaction of leukocytes with ICAM-1 and ICAM-2. Both ICAMs mediate firm adhesion of leukocytes to the endothelium. ICAM-2 is expressed constitutively and is responsible for routine immune surveillance on unstimulated endothelium. ICAM-1 is greatly up-regulated following inflammation, allowing it to mediate most leukocyte adhesion events. It is also involved following injury and aids the body in mounting an immune response. To carry out these different functions, it can be assumed that ICAM-1 and ICAM-2 have different physical properties. Indeed, our whole-cell adhesion studies confirmed that leukocytes bound more strongly to ICAM-1 than to ICAM-2. To further our understanding of the mechanisms involved behind these differences, we performed single-molecule adhesion studies to determine how these interactions behave under external force.

Our single-molecule studies enable us to characterize the intermolecular potential of a receptor–ligand complex. With no applied external force, the dissociation of a complex is governed by its activation energy. Applying an external force adds a linear term to the potential, effectively tilting it and suppressing the energy barrier of the interaction. Suppression of the barrier alters the kinetics of the system. The extent of this change in the dissociation kinetics by the external force depends on the nature of the intermolecular potential of the complex. Hence, determining the force-dependent kinetics of the complex will allow us to identify the shape of the potential.

In our analysis, we assumed that the intermolecular potential is linear as proposed by Bell.[40] According to the Bell model, the energy barrier of a complex is suppressed by $f\gamma$ and the off-rate is given by eq 1. In this model, the potential is characterized by the two parameters, γ and $k°$. Since our technique does not allow us to conveniently apply eq 1 to obtain γ and $k°$, we relied on the dynamic force spectroscopy approach of Evans and Richie.[29] Evans and Ritchie noted that there is a simple expression relating the most probable unbinding of a complex to the loading rate of the unbinding process (eq 3). This approach was used to obtain the shape of the intermolecular potential of the LFA-1/ICAM-1 and LFA-1/ICAM-2 complexes.

In general, the dissociation of a complex involves overcoming multiple energy barriers. An external force will suppress the outer barriers more than the inner barriers. Eventually, at some force, the outer barrier will be energetically lower than the inner barriers and the dissociation rate will then become governed by the properties of the inner barrier. This process continues until all the barriers are overcome.

In the DFS approach, the existence of multiple barriers is revealed by the presence of multiple loading regimes in the force spectrum. Our measurements of the LFA-1/ICAM-1 interaction are consistent with an intermolecular potential consisting of two energy barriers, which we will refer to as the outer and the inner activation barrier. The outer barrier is characterized by the slow loading regime (50–7000 pN/s), and the inner barrier is characterized by the fast loading regime (7000–60 000 pN/s) (Figure 5A). We fit eq 3 to our measurements in order to obtain the Bell model parameters for the two energy barriers of the complex. Table 1 lists the Bell model parameters of the LFA-1/ICAM-1 and LFA-1/ICAM-2 complexes. They provide information regarding the position of the transition state (γ) and the dissociation rate constant in the absence of force ($k°$).

Figure 6A illustrates the intermolecular potential of the LFA-1/ICAM-1 complex. $\Delta G°$ of the high-affinity complex ($15.5k_BT$) was obtained from the equilibrium dissociation rate constant, K_D, of the interaction between the high-affinity open I domain of LFA-1 and ICAM-1, as measured by surface plasmon resonance.[14] Our current study revealed that the dissociation of the LFA-1/ICAM-1 complex involves overcoming an inner and outer barrier with corresponding transition states, TS_1 and TS_2, respectively (Figure 6A). The positions of the

inner and outer barriers of the potential of the high-affinity complexes are 0.56 and 3.5 Å, respectively. This reveals that the complex is stabilized by short-range and intermediate-range interactions as described below.

An estimate of the height of the inner barrier, ΔG_{01}, was obtained from the difference between $\Delta G°$ and ΔG_{12}, the energy difference between the two transition states. ΔG_{12} was calculated using $\Delta G_{12} = -\ k_B T\ \mathrm{In}\left(k_2^\circ / k_1^\circ\right)$, where k_1° and k_2° are the dissociation rate constants of the inner and outer barriers of the high-affinity LFA-1/ICAM-1 complexes, respectively. The ΔG_{12} calculated from the dissociation rate constants of Table 1 was $6.7 k_B T$ for the high-affinity complexes in the ICAM-1 interaction ($3.0 k_B T$ for the low-affinity complexes). Hence, our estimate for the lower limit of ΔG_{01} of the high-affinity LFA-1/ICAM-1 interaction is $8.8 k_B T$, which represents a significant fraction of the total energy difference between the bound and dissociated states of the complex.

To understand the effects of LFA-1 activation on its interaction with ICAM-1, we examined the potential of the low-affinity complex. The differences between the transition-state energies ($\Delta\Delta G$) of the high- and low-affinity (ΔG_H and ΔG_L) LFA-1/ICAM-1 complexes were calculated from $\Delta\Delta G = \Delta G_H - \Delta G_L = -\ k_B T\ \mathrm{In}\left(k_H^\circ / k_L^\circ\right)$, where k_H° and k_L° are the dissociation rate constants of the high- and low-affinity complexes, respectively. For the inner activation barrier, the difference between the high- and low-affinity complexes was negligible, approximately $0.16 k_B T$ (Figure 6A). Based on our analysis, affinity modulation of the LFA-1/ICAM-1 interaction stemmed from a $3.3 k_B T$ elevation of the outer barrier.

The LFA-1/ICAM-2 intermolecular potential also revealed an outer (50–7000 pN/s) and an inner (7000–60 000pN/s) activation barrier (Figure 6B). The positions of the inner and outer barriers of the potential of the high-affinity complexes are 1.5 and 4.9 Å, respectively, resulting in wider and less steep barriers than those observed for the LFA-1/ICAM-1 complex. $\Delta G°$ for the high-affinity complex was calculated to be $14.3 k_B T$ using K_D values for an open I domain binding to ICAM-2 from Shimaoka et al.[14] Our $k°$ values for the inner and outer barriers of the high-affinity LFA-1/ICAM-2 complex are 13 and 0.06 s^{-1}, respectively, which gives a transition-state energy, ΔG_{12}, of $5.4 k_B T$ ($3.5 k_B T$ for the low-affinity complexes). This is a smaller difference than for the LFA-1/ICAM-1 complex, where the height of the second transition state is higher for the high-affinity complex. Based on this value, the calculated ΔG_{01} is greater than $8.9 k_B T$, which is similar to the value obtained for the LFA-1/ICAM-1 interaction. In contrast, the outer activation barrier of the high-affinity complex was calculated to be $1.6 k_B T$ higher than the outer activation barrier of the low-affinity complex, which is 50% less than the difference observed for LFA-1/ICAM-1. This result is consistent with earlier findings that affinity modulation of the LFA-1/ICAM-2 interaction was less effective than the affinity modulation of the LFA-1/ICAM-1 interaction in promoting enhanced adhesion.[41] As with the LFA-1/ICAM-1 interaction, the difference between the inner activation barrier of the high- and low-affinity complexes was small, about $0.26 k_B T$. In summary, the intermolecular potential of the LFA-1/ICAM-2 interaction consists of less steep, wider energy barriers, with smaller differences between the high- and low-affinity states in the outer barrier than seen in the intermolecular potential of the LFA-1/ICAM-1 interaction.

The effects of a pulling force on the dissociation rate of the LFA-1/ICAM-1 and LFA-1/ICAM-2 complexes are summarized by the kinetic profiles of Figure 7. For a two energy barrier model, the dissociation rate is given by

$$k_{\mathrm{off}}(f) = 1/\left\{\left(k_1^\circ\right)^{-1} \exp\left[-f\gamma_1/k_B T\right] + \left(k_2^\circ\right)^{-1} \exp\left[-f\gamma_2/k_B T\right]\right\} \quad (4)$$

where the indices in the subscript of the Bell model parameters, γ and $k°$, refer to the inner (1) and outer (2) barriers. At low pulling forces, the dissociation rate is governed by the properties of the outer barrier, γ_2 and k_2°. In all cases there is a fast exponential increase in the off-rate, which becomes more gradual for pulling forces greater than ~80 pN for the LFA-1/ICAM-1 interaction and ~60 pN for the LFA-1/ICAM-2 interaction. At these higher pulling forces, the outer barriers of the complexes are suppressed and the dissociation rates are governed by the properties of the steep inner activation barriers, which make the off-rate less responsive to a pulling force. With the exception of very low pulling forces, the LFA-1/ICAM-1 interaction resists pulling forces better than the LFA-1/ICAM-2 interaction.

Following the activation of LFA-1, both complexes are able to resist pulling forces better at lower forces, <70 pN for the LFA-1/ICAM-2 complex and <110 pN for the LFA-1/ICAM-1 complex (Figure 7). These differences are due to the elevation of the outer barrier by $3.3k_BT$ for the ICAM-1 complex and by $1.6k_BT$ for the ICAM-2 complex following LFA-1 activation. The magnitude of the difference in the energy of the barriers determines the difference seen between the off-rate of the high-and low-affinity complexes. For example, at a pulling force of 30 pN, the difference between the high- and low-affinity LFA-1/ICAM-1 complex was ~12-fold and only ~3-fold for LFA-1/ICAM-2 complex. At higher pulling forces, the dissociation rates are governed by the inner barriers, which were unaffected by the activation of LFA-1. Hence, there is no difference between the high- and low-affinity-state complexes.

The ICAM-2 complex is much less resistant to a pulling force than the ICAM-1 complex, as is evident by the slopes of the kinetic profiles (Figure 7). This slope is largely determined by the width of the energy barriers, γ. A larger γ would give rise to a steeper slope in the kinetic profile, making the complex less resistant to a pulling force. Both barriers of the ICAM-2 complex are wider than those of the ICAM-1 complex (Table 1), leading to an overall steeper slope in its kinetic profile. In addition, the ICAM-2 complex has an outer barrier that is ~3 Å wider than the inner barrier. This leads to a steeper slope in the kinetic profile for lower pulling forces (<60 pN for the low-affinity complex) and a less steep slope for the higher pulling forces. ICAM-1 also has a wider outer barrier (~2 Å difference), resulting in a steeper slope for lower pulling forces (<80 pN for the low-affinity complex) and a less steep slope at the higher forces.

Differences in the kinetic profiles and intermolecular potentials of ICAM-1 and ICAM-2 can be attributed to structural differences in their binding site. In both cases binding of LFA-1 involves the interaction of the I domain of LFA-1 with the first Ig domain of ICAM-1 and ICAM-2. Moreover, both ICAM-1 and ICAM-2 contribute a glutamic acid residue to the coordination of the Mg^{2+} ion that is chelated to the MIDAS of the I domain. This hydrophilic glutamic acid (Glu-34 in ICAM-1 and Glu-37 in ICAM-2) is surrounded by a ring of hydrophobic amino acids that interacts with a complementary hydrophobic ring on the I domain of LFA-1. Mutational studies of the amino acids found in these rings reveal potentially significant differences which may impact both the binding strength as well as the off-rate. The hydrophobic residues on ICAM-1 that surround Glu-34 are Pro-36, Tyr-66, Met- 64, and the aliphatic portions of Gln-62 and Gln-73.[13] Furthermore, Met-140 on the I domain protrudes and inserts its side chain into a shallow cleft between Met-64 and Pro-36 on ICAM-1.[13,42]

A similar hydrophobic ring, which includes Ser-39, His-68, Val-64, and Gln-75, surrounds Glu-37 of ICAM-2. However, in the structure of ICAM-2, Gln-66, a much more polar and less hydrophobic residue is present in place of Met-64.[9,43] Unlike the Met-64 in ICAM-1, mutation of Gln-66 in ICAM-2 has no effect on LFA-1 binding.[10] Thus, the higher k_{off} values for the LFA-1/ICAM-2 interaction can be attributed to the weaker interaction between hydrophobic rings of the ICAM-2/LFA-1 complex. In addition, since the hydrophobic ring in ICAM-2 is less well-packed, the binding interface of ICAM-2 is not as flat as that of ICAM-1.[44,45] This may give rise to the more diffused of the LFA-1/ICAM-2 interaction.

The kinetic data presented in this study are consistent with the physiological functions of both ICAM-1 and ICAM-2. Two-thirds of leukocyte adhesion to resting endothelium is mediated by ICAM-2 and the rest by ICAM-1.[46] ICAM-2 is therefore more important in the unstimulated state, but ICAM-1 is essential during inflammation, when its expression levels are up-regulated approximately 40-fold.[5,7,47] The interaction of ICAM-2 with LFA-1 is weaker and less resistant to pulling forces than the LFA-1/ICAM-1 interaction. This results in less overall leukocyte adhesion and allows ICAM-2 to carry out its function of routine immune surveillance. In addition, our kinetic data reveal that LFA-1 affinity modulation only moderately enhances adhesion to ICAM-2, while it greatly enhances adhesion to ICAM-1. Therefore, ICAM-1 appears to be well-suited for eliciting strong and specific leukocyte adhesion during inflammation and in mounting an immune response.

We conclude that the DFS for the unbinding of LFA-1 from both ICAM-1 and ICAM-2 involves overcoming two activation barriers. The steep inner barrier, which allows complexes to resist pulling forces, is considerably steeper for the ICAM-1 interaction. The outer barrier determines the height of the high-affinity state of both interactions. This barrier is also steeper for ICAM-1, and the difference between the high- and low-affinity states is twice as great for LFA-1/ICAM-1 as compared to the LFA-1/ICAM-2 complex. Therefore, the ICAM-1 interaction is more stable and exhibits stronger binding to the high-affinity form of LFA-1. Differences in the hydrophobicity of the amino acids which surround the key glutamic acid residues in the LFA-1 binding sites on the ICAMs support these observations. The reported differences in kinetics also reflect the physiological roles of both ICAMs. ICAM-2 expression is constitutive and considerably higher than ICAM-1 on unstimulated endothelium, when binding to low-affinity LFA-1 is most likely to occur. ICAM-1 expression is dominant during inflammation when activated LFA-1 is most likely to be present.

Acknowledgment

This work was supported in part by grants from the American Heart Association, the National Science Foundation, Biomedical Interaction Technologies Center, and the National Institute of Health (Grant GM55611). We would like to thank C. Freites for technical support and H. Azad for help with this work.

References and Notes

1. Huang MT, Mason JC, Birdsey GM, Amsellem V, Gerwin N, Haskard DO, Ridley AJ, Randi AM. Blood 2005;106:1636–1643. [PubMed: 15920013]
2. Hynes RO. Cell 1992;69:11–25. [PubMed: 1555235]
3. Issekutz AC, Rowter D, Springer TA. J. Leukocyte Biol 1999;65:117–126. [PubMed: 9886254]
4. Shang XZ, Issekutz AC. Eur. J. Immunol 1998;28:1970–1979. [PubMed: 9645379]
5. Lehmann JC, Jablonski-Westrich D, Haubold U, Gutierrez-Ramos JC, Springer T, Hamann A. J. Immunol 2003;171:2588–2593. [PubMed: 12928410]
6. Xu H, Bickford JK, Luther E, Carpenito C, Takei F, Springer TA. J. Immunol 1996;156:4909–4914. [PubMed: 8648141]
7. Dustin ML, Springer TA. J. Cell Biol 1988;107:321–331. [PubMed: 3134364]
8. Staunton DE, Dustin ML, Springer TA. Nature 1989;339:61–64. [PubMed: 2497351]
9. Casasnovas JM, Pieroni C, Springer TA. Proc. Natl. Acad. Sci. U.S.A 1999;96:3017–3022. [PubMed: 10077629]
10. Staunton DE, Dustin ML, Erickson HP, Springer TA. Cell 1990;61:243–254. [PubMed: 1970514]
11. Wang J, Springer TA. Immunol Rev 1998;163:197–215. [PubMed: 9700512]
12. Stanley P, McDowall A, Bates PA, Brashaw J, Hogg N. Biochem. J 2000;351:79–86. [PubMed: 10998349]
13. Shimaoka M, Xiao T, Liu JH, Yang Y, Dong Y, Jun CD, McCormack A, Zhang R, Joachimiak A, Takagi J, Wang JH, Springer TA. Cell 2003;112:99–111. [PubMed: 12526797]

14. Shimaoka M, Lu C, Palframan RT, von Andrian UH, McCormack A, Takagi J, Springer TA. Proc. Natl. Acad. Sci. U.S.A 2001;98:6009–6014. [PubMed: 11353828]
15. Woska JR Jr. Morelock MM, Jeanfavre DD, Bormann BJ. J. Immunol 1996;156:4680–4685. [PubMed: 8648112]
16. Lollo BA, Chan KW, Hanson EM, Moy VT, Brian AA. J. Biol. Chem 1993;268:21693–21700. [PubMed: 8104943]
17. Lupher ML Jr. Harris EA, Beals CR, Sui LM, Liddington RC, Staunton DE. J. Immunol 2001;167:1431–1439. [PubMed: 11466362]
18. Stewart M, Hogg N. J. Cell Biochem 1996;61:554–561. [PubMed: 8806078]
19. van Kooyk Y, Figdor CG. Curr. Opin. Cell Biol 2000;12:542–547. [PubMed: 10978887]
20. Kuhlman P, Moy VT, Lollo BA, Brian AA. J. Immunol 1991;146:1773–1782. [PubMed: 1672331]
21. Benoit M, Gabriel D, Gerisch G, Gaub HE. Nat. Cell Biol 2000;2:313–317. [PubMed: 10854320]
22. Heinz WF, Hoh JH. Trends Biotechnol 1999;17:143–150. [PubMed: 10203772]
23. Willemsen OH, Snel MM, Cambi A, Greve J, De Grooth BG, Figdor CG. Biophys. J 2000;79:3267–3281. [PubMed: 11106630]
24. Zhang X, Wojcikiewicz E, Moy VT. Biophys. J 2002;83:2270–2279. [PubMed: 12324444]
25. Wojcikiewicz EP, Zhang X, Moy VT. Biol. Proced. Online 2004;6:1–9. [PubMed: 14737221]
26. Hutter J, Bechhoefer J. Rev. Sci. Instrum 1993;64:1868–1873.
27. Tees DF, Waugh RE, Hammer DA. Biophys. J 2001;80:668–682. [PubMed: 11159435]
28. Ahmed N, Nino DF, Moy VT. Rev. Sci. Instrum 2001;72:2731–2734.
29. Evans E, Ritchie K. Biophys. J 1997;72:1541–1555. [PubMed: 9083660]
30. Stewart MP, Cabanas C, Hogg N. J. Immunol 1996;156:1810–1817. [PubMed: 8596031]
31. Labadia ME, Jeanfavre DD, Caviness GO, Morelock MM. J. Immunol 1998;161:836–842. [PubMed: 9670961]
32. Berry N, Ase K, Kikkawa U, Kishimoto A, Nishizuka Y. J. Immunol 1989;143:1407–1413. [PubMed: 2474594]
33. Rothlein R, Springer TA. J. Exp. Med 1986;163:1132–1149. [PubMed: 3517218]
34. Pyszniak AM, Welder CA, Takei F. J. Immunol 1994;152:5241–5249. [PubMed: 7910620]
35. Wojcikiewicz EP, Zhang X, Chen A, Moy VT. J. Cell Sci 2003;116:2531–2539. [PubMed: 12734401]
36. Li F, Redick SD, Erickson HP, Moy VT. Biophys. J 2003;84:1252–1262. [PubMed: 12547805]
37. Zhang X, Craig SE, Kirby H, Humphries MJ, Moy VT. Biophys. J 2004;87:3470–3478. [PubMed: 15347595]
38. Evans E. Annu. Rev. Biophys. Biomol. Struct 2001;30:105–128. [PubMed: 11340054]
39. Merkel R, Nassoy P, Leung A, Ritchie K, Evans E. Nature 1999;397:50–53. [PubMed: 9892352]
40. Bell GI. Science 1978;200:618–627. [PubMed: 347575]
41. Binnerts ME, van Kooyk Y, Simmons DL, Figdor CG. Eur. J. Immunol 1994;24:2155–2160. [PubMed: 7916295]
42. Casasnovas JM, Stehle T, Liu JH, Wang JH, Springer TA. Proc. Natl. Acad. Sci. U.S.A 1998;95:4134–4139. [PubMed: 9539702]
43. Casasnovas JM, Springer TA, Liu JH, Harrison SC, Wang JH. Nature 1997;387:312–315. [PubMed: 9153399]
44. Song G, Lazar GA, Kortemme T, Shimaoka M, Desjarlais JR, Baker D, Springer TA. J. Biol. Chem 2006;281:5042–5049. [PubMed: 16354667]
45. Song G, Yang Y, Liu JH, Casasnovas JM, Shimaoka M, Springer TA, Wang JH. Proc. Natl. Acad. Sci. U.S.A 2005;102:3366–3371. [PubMed: 15728350]
46. Xu H, Gonzalo JA, St Pierre Y, Williams IR, Kupper TS, Cotran RS, Springer TA, Gutierrez-Ramos JC. J. Exp. Med 1994;180:95–109. [PubMed: 7911822]
47. de Fougerolles AR, Stacker SA, Schwarting R, Springer TA. J. Exp. Med 1991;174:253–267. [PubMed: 1676048]
48. Evans E, Leung A, Hammer D, Simon S. Proc. Natl. Acad. Sci. U.S.A 2001;98:3784–3789. [PubMed: 11274395]

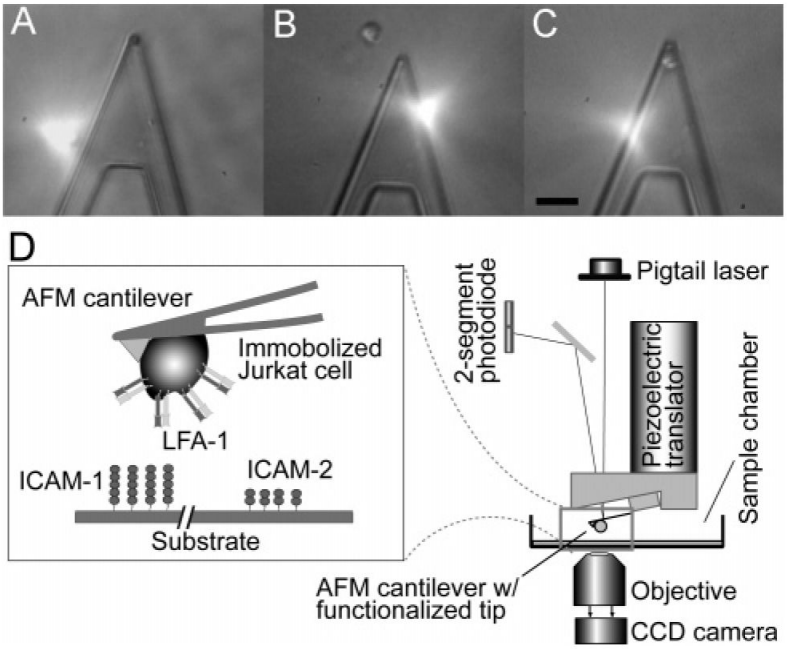

Figure 1.

(A) AFM cantilever. (B) AFM cantilever approaching Jurkat T cell. (C) AFM cantilever with Jurkat T cell attached via concanavalin-A linkage. The bar is 30 μm. (D) Schematic of the AFM setup. The experimental system is shown in the inset. A Jurkat cell was attached to the AFM cantilever and allowed to interact with the protein-coated cell culture dish.

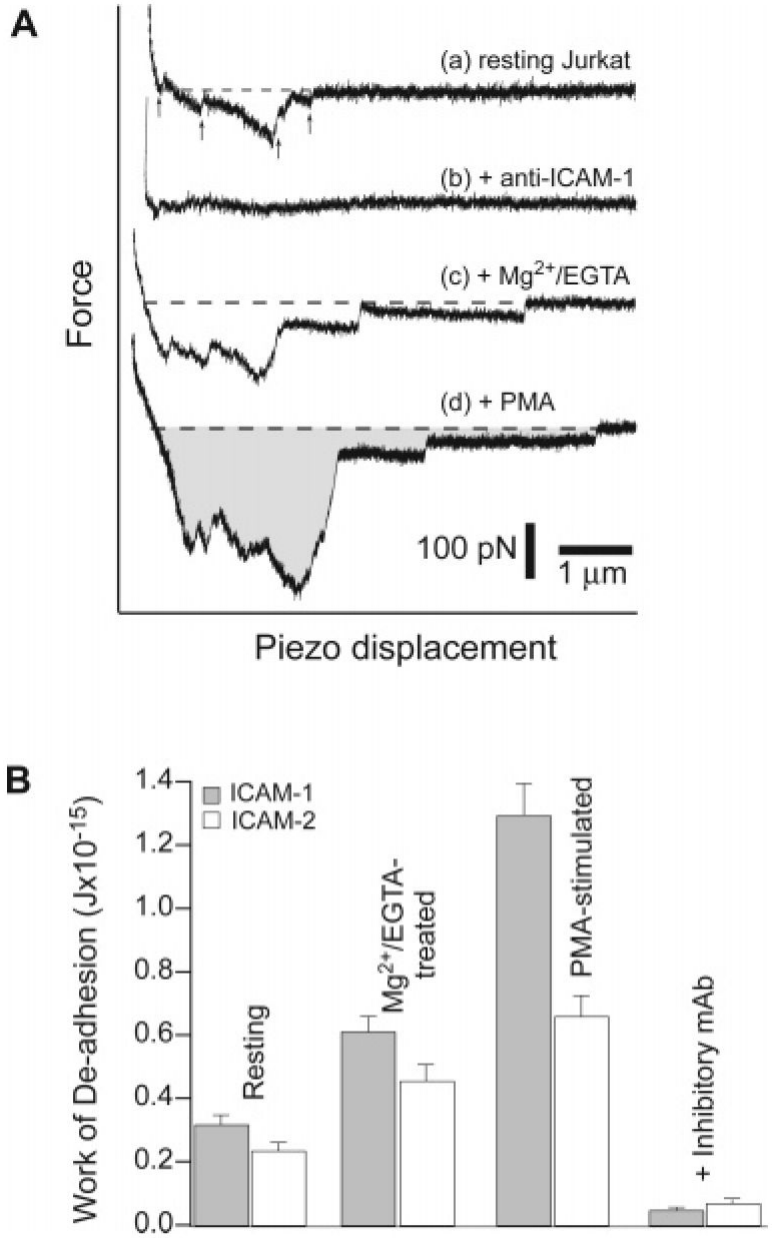

Figure 2.

(A) AFM force-displacement measurements of the interaction between a Jurkat cell and immobilized ICAM-1. Traces a and b record the interaction between a resting Jurkat cell and ICAM-1 under normal condition and in the presence of an anti-ICAM-1 mAb (BBIG-I1, 50 μg/mL), respectively. For traces c and d, the cells were activated by Mg^{2+}/EGTA (5 mM, 1 mM) and PMA (100 nM), respectively. The measurements were acquired with 200 pN indentation force, 3 s contact time, and a cantilever retraction speed of 5 μm/s. The shaded area in the bottom trace indicates the "work of de-adhesion". Arrows in the top trace point to rupture events, i.e., breakage of adhesive bond(s). Dashed lines mark the position of zero force for each measurement. (B) Work of de-adhesion for the detachment of Jurkat cell interaction with ICAM-1 (gray bars) and ICAM-2 (white bars). The error bars represent the standard error.

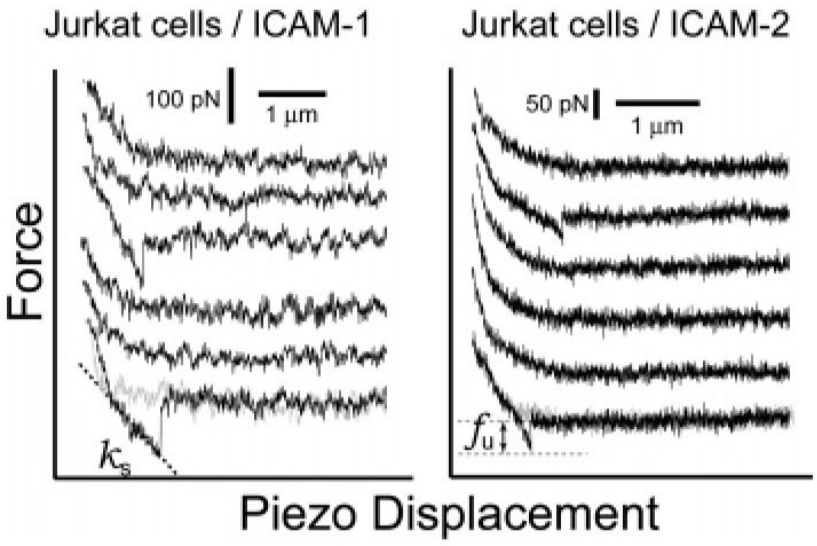

Figure 3.
Sample force-displacement traces of unitary LFA-1/ICAM-1 (A) and LFA-1/ICAM-2 (B) unbinding forces. Both sets of measurements were acquired at speeds of 5 μm/s and conditions that minimized contact (~50 ms contact time and ~100 pN indentation force) ensuring an adhesion frequency of less than 30%. Adhesion was observed in the third and sixth traces in panel A and the second and sixth traces in panel B. f_u is the unbinding force of the interaction, and k_s is the system spring constant derived from the slope of the force-displacement graph.

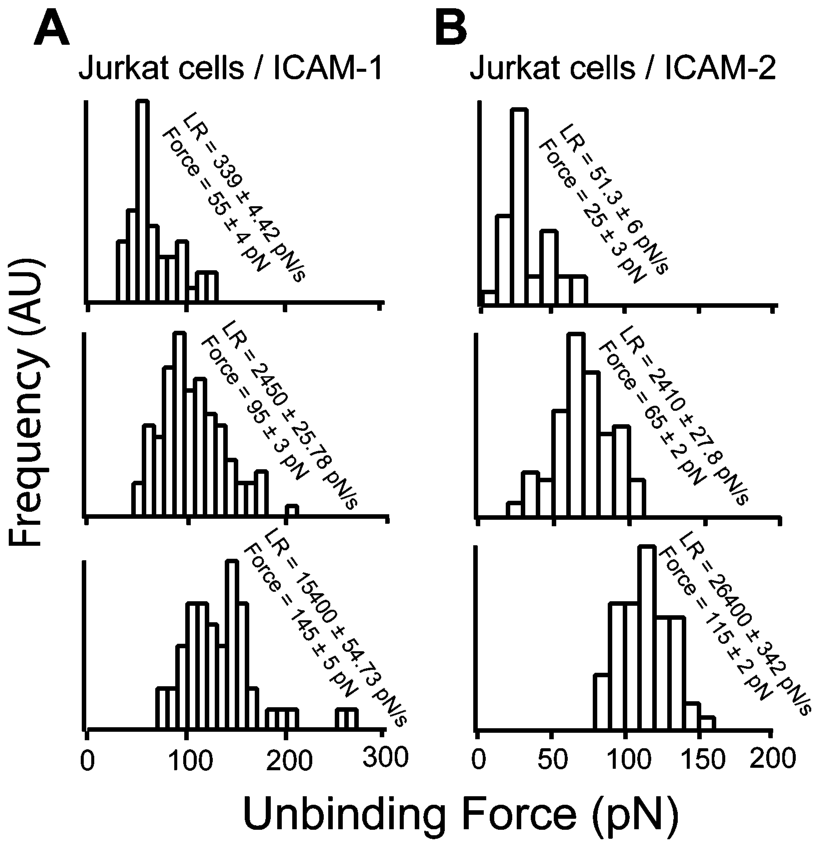

Figure 4.
Histograms of breakage forces of individual LFA-1/ICAM-1 and LFA-1/ICAM-2 unbinding forces from the force-displacement traces of Jurkat cells and ICAM-1 (A) and ICAM-2 (B). The breakage forces were derived from the magnitude of the force transitions acquired in measurements obtained with a compression force of ~100 pN, ~50 ms contact, and increasing loading rates. The *y*-axis plots the number of force transitions detected. The error bars represent the standard error.

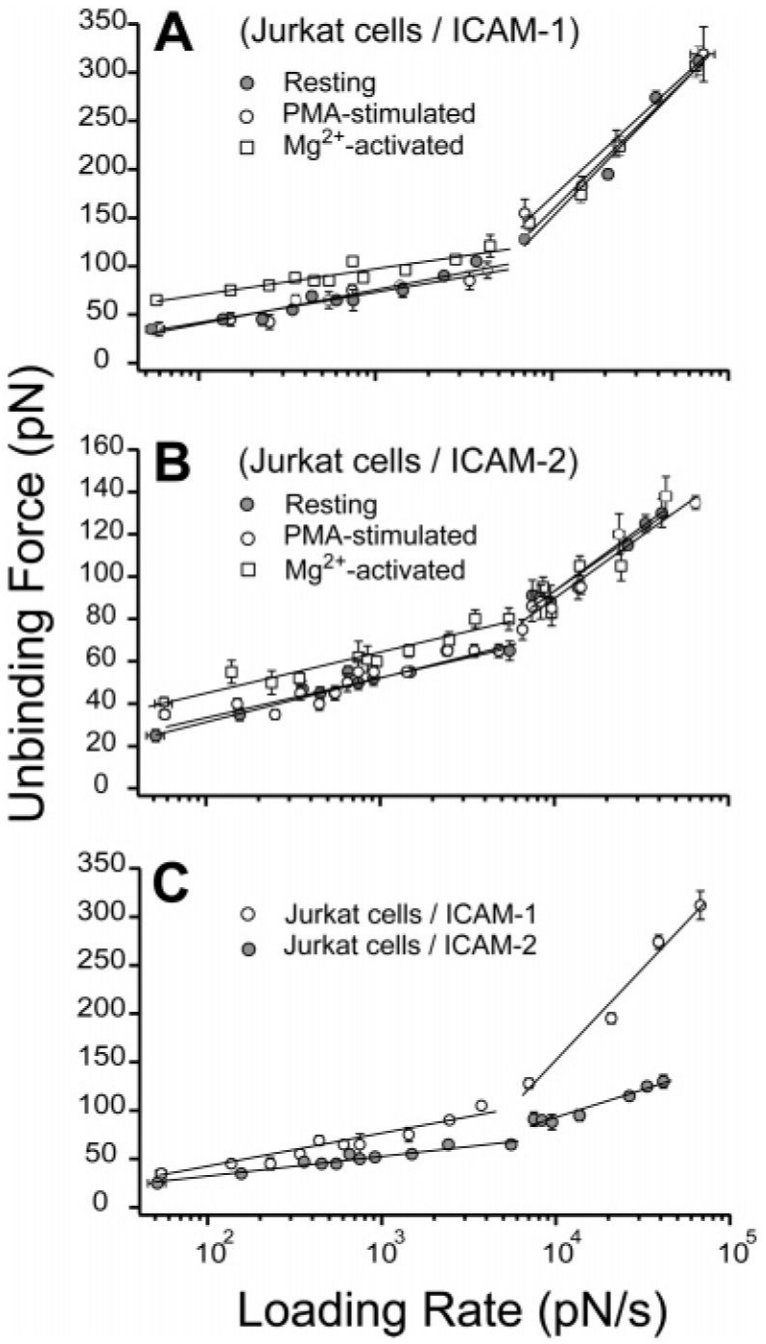

Figure 5.

Dynamic force spectrum (DFS) of the LFA-1/ICAM-1 and LFA-1/ICAM-2 interactions. Measurements were acquired at a loading rate range of 50–60 000 pN/s, which was achieved by varying the retraction rate of the cantilever from 0.1 to 26 μm/s. Forces acquired at cantilever retraction speeds > 1 μm/s were corrected for hydrodynamic drag.[48] All forces were grouped according to loading rate. The most probable unbinding forces were taken from the mode of the unbinding force histograms or the histogram peak. The linear fits were obtained using eq 3. (A) The LFA-1/ICAM-1 interaction was measured under three different experimental conditions: resting cells (filled circle), PMA-stimulated cells (open circle), and Mg^{2+}-treated cells (square). (B) Three different conditions also represented for the LFA-1/ICAM-2

interaction: resting cells (filled circle), PMA-stimulated cells (open circle), and Mg^{2+}-treated cells (square). (C) Comparison of the adhesion of resting Jurkat cell to ICAM-1 (open circles) and ICAM-2 (filled circles). The error bars represent the standard error.

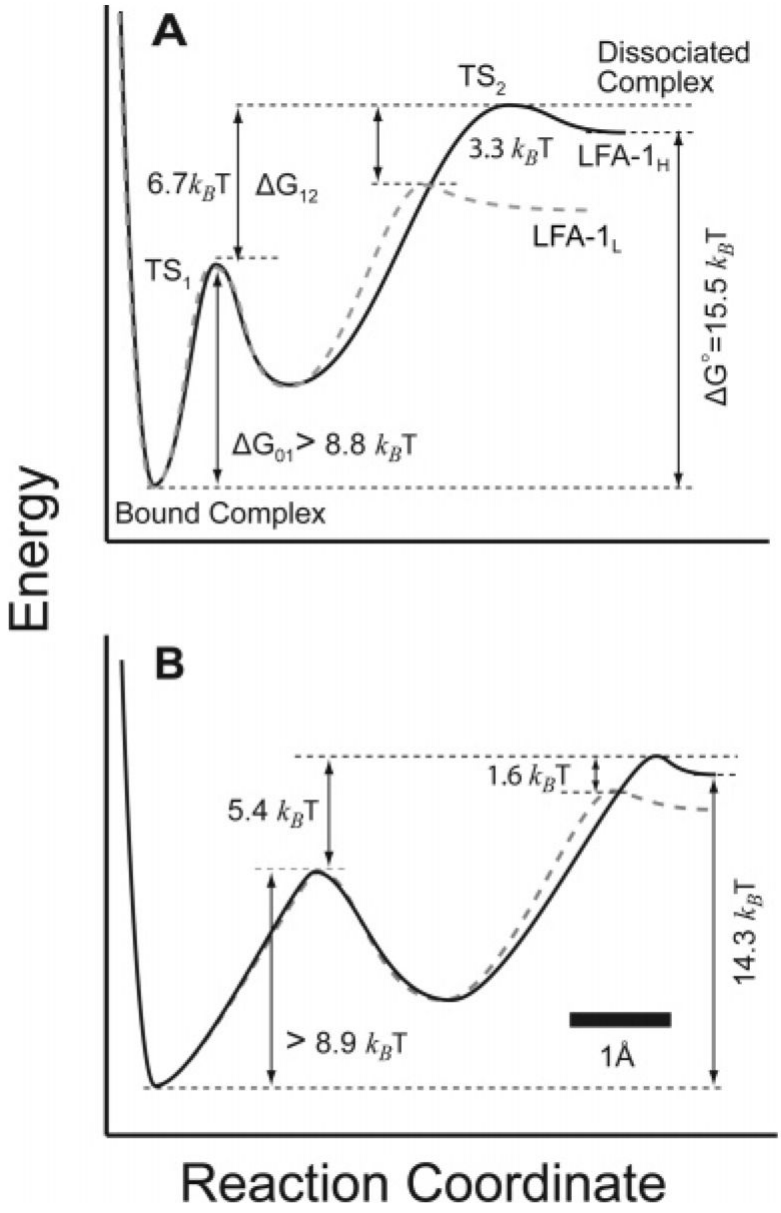

Figure 6.

Intermolecular potentials of the human LFA-1/ICAM-1 (A) and LFA-1/ICAM-2 (B) interactions. Estimates of the equilibrium free energies ($\Delta G°$) were derived from the equilibrium affinity constants reported in Shimaoka et al.[14] (A) Two transition states (TS_1 and TS_2) were observed in the dissociation of high- (black trace) and low-affinity (dashed, gray trace) LFA-1 from ICAM-1. $\Delta G°$ was calculated to be 15.5 k_B T. The difference between TS_1 and TS_2 was 6.7 k_B T. The inner activation barriers of the high- and low-affinity complexes were >8.8 k_B T. The difference between the high- and low-affinity complexes was 3.3 k_B T. (B) Two transition states were also present in the dissociation of high- (black trace) and low-affinity (dashed, gray trace) LFA-1 from ICAM-2. $\Delta G°$ was calculated to be 14.3 k_B T. The difference between TS_1 and TS_2 was 5.4 k_B T. The inner activation barriers of the high- and low-affinity complexes were >8.9 k_B T. The difference between the high- and low-affinity complexes was 1.6 k_B T.

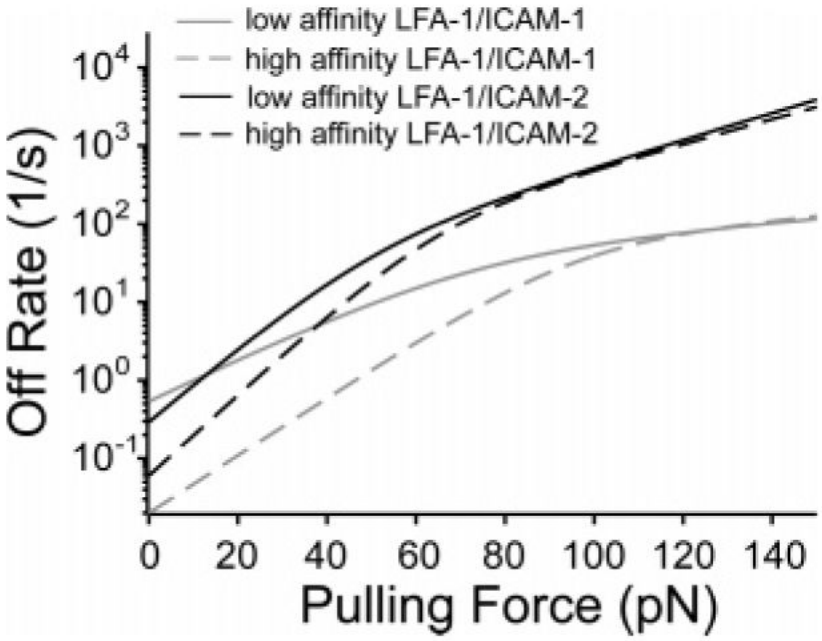

Figure 7.
Kinetic profiles for LFA-1/ICAM-1 and LFA-1/ICAM-2 interactions. The solid lines represent unactivated, low-affinity LFA-1 on resting Jurkat cells, and the dashed lines, high-affinity LFA-1 complexes on activated Jurkat cells. Equation 4 provides the force-dependent dissociation rate of the complexes.

Table 1

Bell Model Parameters of the LFA-1/ICAM-1 and LFA-1/ICAM-2 Interactions[a]

	conditions	γ_1 (Å)	$k_1^\circ(s^{-1})$	γ^2 (Å)	$k_2^\circ(s^{-1})$
LFA-1/ICAM-1	resting	0.49	19	2.6	0.55
	PMA	0.56	13	2.9	0.41
	Mg^{2+}/EGTA	0.56	17	3.5	0.02
LFA-1/ICAM-2	resting	1.6	10	4.5	0.31
	PMA	1.6	12	5.0	0.18
	Mg^{2+}/EGTA	1.5	13	4.9	0.06

[a]The Bell model parameters were calculated in Igor Pro software using eq 3. Values for the inner and outer barrier are represented by indices 1 and 2, respectively.